Publications of the Astronomical Society of the Pacific
108: 580–590, 1996 July

36 Ophiuchi AB: Incompatibility of the Orbit and Precise Radial Velocities

ALAN W. IRWIN AND STEPHENSON L. S. YANG[1]

Department of Physics and Astronomy, University of Victoria, P. O. Box 3055, Victoria, British Columbia, Canada, V8W 3P6
Electronic mail: irwin@uvastro.phys.uvic.ca, yang@uvastro.phys.uvic.ca

GORDON A. H. WALKER[1]

Department of Geophysics and Astronomy, University of British Columbia, Vancouver, British Columbia, Canada, V6T 1Z4
Electronic mail: walker@astro.ubc.ca

Received 1994 December 8; accepted 1996 April 11

ABSTRACT. The long-period (~600 yr) binary system 36 Ophiuchi AB consists of two chromospherically active K dwarfs. If we constrain the period using the mass–luminosity relation and the observed parallax, the remaining orbit parameters can be estimated from the 170 years of visual-binary observations. In this paper, we further constrain the orbit by precise measurements of the differential radial velocities (with arbitrary zero points) of both 36 Oph A and B and the difference in radial velocity between 36 Oph B and A. Our best orbit gives a good fit to the visual-binary observations, the difference in velocity, and the mean radial acceleration of A; but the observed acceleration of B is a factor of 1.64 larger than the value predicted by the orbit. This factor is so large that no reasonable variation in the adopted sum of masses, mass ratio, parallax, or orbit parameters will remove the B acceleration discrepancy. The maximum companion mass allowed by the residuals from the visual-binary orbit is of order 8 Jupiter masses for assumed periods between 30 and 100 yr so the 36 Oph B acceleration discrepancy would ordinarily make it a candidate for a substellar companion. However, the very high eccentricity (~0.9) of the binary-star orbit means its closest approach is of order 6 a.u., making it unlikely that any substellar companions would form or survive with semi-major axis exceeding ~1.5 a.u. or period exceeding ~2 yr. Thus, 36 Oph B is an important counter-example which serves as a warning that for chromospherically active stars, at least, it is possible to have apparent radial accelerations in the absence of substellar companions.

1. INTRODUCTION

As part of a twelve-year program completed in 1992 at the Canada–France–Hawaii Telescope (CFHT), we monitored the precise radial velocity (PRV) of several binary systems. This paper is the third in a series discussing the additional constraints placed on binary orbits by our PRV data. In Papers I and II (Irwin et al. 1992a,b), we have rediscussed the orbits of χ^1 Orionis and Procyon. In the present paper, we turn our attention to the orbit of 36 Ophiuchi AB.

36 Oph is actually a triple system. The components are A (=HR 6402=HD 155886 with $\alpha = 17^h15^m20^s.8$, $\delta = -26°36'05''$; J2000); B (=HR 6401=HD 155885 with $\alpha = 17^h15^m21^s.0$, $\delta = -26°36'10''$; J2000); and C (K5 V) which is a common-proper-motion companion separated by 700 arcsec from AB (Hoffleit and Warren 1991). Although the three stars in this system provide important tests of abundance work and stellar interior theory (Cayrel de Strobel et al. 1989), we ignore 36 Oph C in the remainder of this paper because it has a negligible effect on the motions of the 36 Oph AB binary (currently separated by 4.6 arcsec and designated 36 Oph through the remainder of this paper).

36 Oph is a long-period (~600 yr) binary system made up of two chromospherically active K dwarfs with virtually identical characteristics (A: $V = 5.07$, $B-V = 0.85$, and SpT=K0 V; B: $V = 5.11$, $B-V = 0.86$, and SpT=K1 V; Hoffleit and Warren 1991). The cataloged orbit (Orbit 1 of this paper taken from Orbit II of Brosche 1960) was classified as "indeterminate" (Worley and Heintz 1991) because the period could not be determined from observations alone. However, for long-period binaries with relatively well-determined parallaxes such as 36 Oph, it is possible to estimate the period from the parallax and mass–luminosity relation. This was done for Orbit 1, and the results must therefore have some degree of reliability within the uncertainties of the parallax and mass–luminosity relation. However, when we compare the predictions of Orbit 1 with our PRV results for 36 Oph A and B, we find agreement for A, but the observed acceleration of B is a factor of 1.56 larger than the value predicted by the orbit (see Table 1). In the current paper we use new observations to improve upon Orbit 1, and we show that orbital uncertainties are unlikely to be the cause of the radial-acceleration discrepancy.

2. THE PRECISE RADIAL VELOCITIES

We determine the PRV results from spectra which are typically observed with S/N>1000 per pixel in the continuum. Systematic shifts due to instrumental effects are calibrated (Campbell and Walker 1979) by observing the stellar

[1]Visiting Astronomer, Canada–France–Hawaii Telescope, operated by the National Research Council of Canada, the Centre National de la Recherche Scientifique of France, and the University of Hawaii.

TABLE 1
Observed Accelerations and Residuals

	Observed[a]		Calculated[b] for Orbit Number				O–C[c] for Orbit Number			
Star	Value	Error	1	2	3	4	1	2	3	4
A	750	170	680	884	928	646	70	−134	−178	104
B	−1060	130	−680	−884	−928	−646	−380	−176	−132	−414
B–A	−1810	210	−1361	−1769	−1855	−1292	−449	−41	45	−518

Notes to TABLE 1

[a]The slope and its formal error are derived from a weighted fit to the observed radial velocities.
[b]Calculated acceleration, where the calculated orbits are described in Table 4 and the text.
[c]Calculated acceleration residual.
All accelerations are in units of m s^{-1} Jcy^{-1}.

spectra through a hydrogen fluoride (HF) absorption cell. The technique has proved stable for more than a decade with errors that are of order 15 m s^{-1}.

Our spectral observations of 36 Oph A and B were obtained with the HF absorption cell and *f*/8.2 coudé spectrograph at the Canada–France–Hawaii 3.6-m telescope. The two stars are currently separated by 4.6 arcsec and, therefore, are easily distinguished in the good seeing conditions (typically less than 1 arcsec) at the CFHT.

We determine relative radial velocities from the 36 Oph A and B spectra largely following the published reduction procedure (Campbell, Walker, and Yang 1988 and references therein). The data are automatically corrected for the secular acceleration due to the proper motion of the stars. Our algorithm, which should be correct to all orders in the space motion, agrees well with the first-order result given by van de Kamp [1981, Eq. (8.18)], 20 m s^{-1} Jcy^{-1}. [Throughout this paper the unit of a Julian century (≡36525 dy) is designated Jcy.] We calculate the internal errors (standard deviation of the mean) of the mean radial velocities from the standard deviation of individual line values. The average internal errors of the 36 Oph A and 36 Oph B velocities are 14

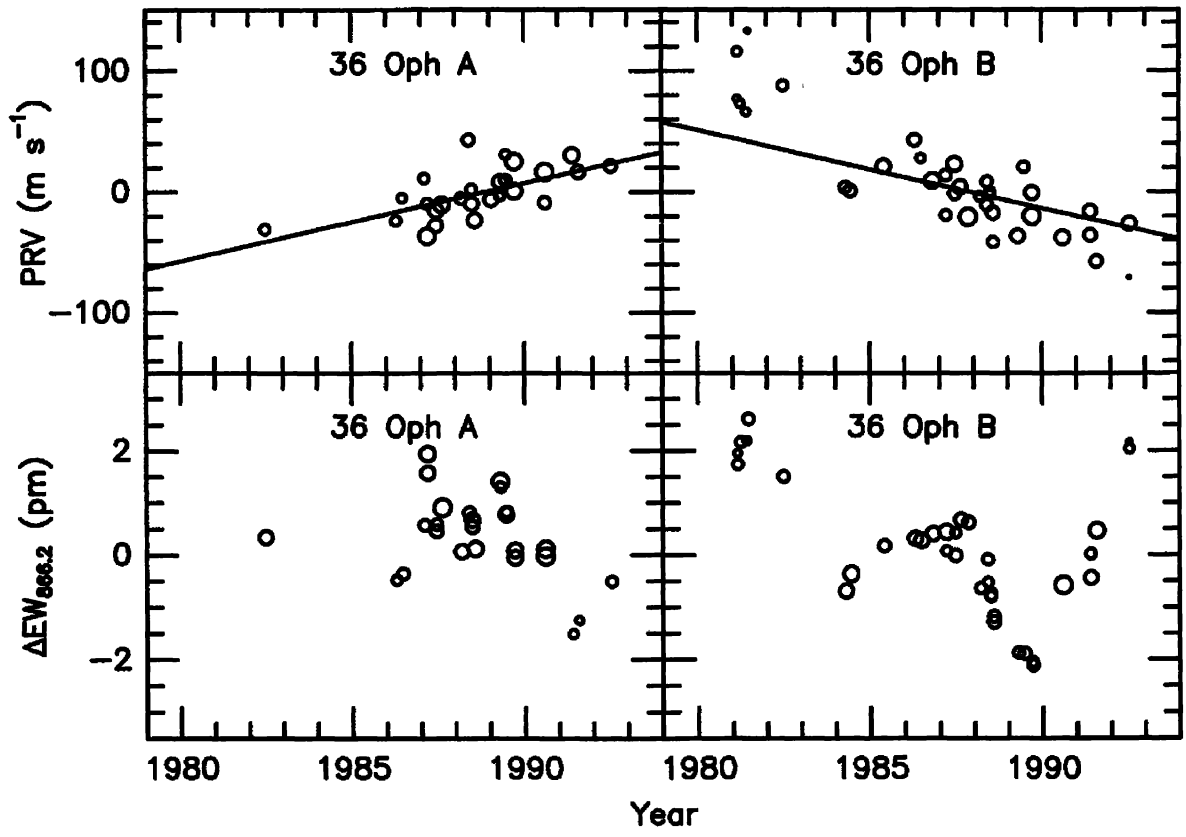

FIG. 1—The precise radial velocity and index of chromospheric activity $\Delta EW_{866.2}$ for 36 Oph A and B. The PRV data are *differential* with the weighted mean velocity arbitrarily set to zero for each of the stars. In contrast, the two $\Delta EW_{866.2}$ plots have a common zero point. For each data point, the area of the circle is proportional to the weight. The average PRV internal errors are (A) 14 and (B) 17 m s^{-1}. The average $\Delta EW_{866.2}$ internal errors are (A) 0.07 and (B) 0.08 pm. We show the Orbit 4 (see Table 4) predictions as solid lines in the PRV plots.

TABLE 2
Observed Velocity Differences and Residuals

Year	RJD[c]	Observed[a] Value	Observed[a] Error	O–C[b] for Orbit Number 1	2	3	4
1987.2	6865.12	661	22	1560	1867	2129	4
1991.4	8405.94	604	15	1561	1886	2151	−1

Notes to TABLE 2

[a]ΔV_{B-A}, the difference in radial velocity between B and A. The error in ΔV_{B-A} is determined from the internal errors of the appropriate A and B velocities.
[b]Calculated residuals in ΔV_{B-A} where the calculated orbits are described in Table 4 and the text.
[c]$JD - 2440000$ in units of dy.
All velocities are in units of m s^{-1}. If one accounts for the observed accelerations of A and B (see Table 1), the two observed ΔV_{B-A} values agree within their errors. Also, Orbit 4 is the only orbit that fits the observed ΔV_{B-A} values.

and 17 m s^{-1}, respectively. We apply corrections to the PRV data to compensate for systematic offsets in the collective differential velocities between observing runs (Larson et al. 1993b). These observing run corrections are usually 15 m s^{-1} or less.

Figure 1 illustrates the PRV results for both 36 Oph A and B. These data (Walker et al. 1995, hereafter WWILYR) are archived with NSSDC/ADC [the (United States) National Space Science Data Center/Astronomical Data Center]. (Electronic access to the NSSDC/ADC catalogs can be obtained from URL = http://adc.gsfc.nasa.gov/.) The PRV data are *differential* with the weighted mean arbitrarily set to zero for each star. Both stars show opposite PRV accelerations that are characteristic of spectroscopic-binary variations. Table 1 gives the mean accelerations derived from the PRV results. The orbit predictions given in Fig. 1 and Table 1 will be discussed below.

Figure 1 also illustrates $\Delta EW_{866.2}$, our index of Ca II core emission and a measure of chromospheric activity (Larson et al. 1993a). Note that the differential measures of $\Delta EW_{866.2}$ for 36 Oph A and B are plotted in Fig. 1 using a common zero point (see next section). Clearly, both stars are chromospherically active with 36 Oph B showing long-term activity that is characteristic of stellar cycles, and 36 Oph A showing more complicated behavior that includes enhanced short-term activity.

3. THE VELOCITY DIFFERENCE ΔV_{B-A} BETWEEN 36 OPH B AND 36 OPH A

The difference in the radial velocity between 36 Oph B and A, ΔV_{B-A}, is an important constraint on the orbit (see below). However, the random errors of published radial velocities often exceed 1 km s^{-1} because of low S/N and resolution. Probably the Fick Observatory radial-velocity scanner results (Beavers and Eitter 1986) are the best of the published material. From the ten nights where they determined the radial velocity of both 36 Oph A and B with their highest ("A") quality observations we derive individual ΔV_{B-A} values which should have systematic errors due to instrumental effects minimized. From these data, we derive a mean value (and formal error of that mean) of $\Delta V_{B-A} = 550 \pm 460$ m s^{-1}. The epochs of the individual data ranged from 1978.2 through 1983.5.

A slight modification of our usual PRV reduction technique allows the determination of ΔV_{B-A} for 36 Oph with greatly improved precision compared to the literature values. (The modified reduction also allows us to determine the $\Delta EW_{866.2}$ results for 36 Oph A and B using a common zero point.) We simply insert the highest S/N spectrum of 36 Oph B (+HF) in the usual PRV reduction of all the 36 Oph A (+HF) spectra, and we determine ΔV_{B-A} using the difference of the derived B velocity relative to the velocity from an A (+HF) spectrum observed within an hour of the B (+HF) spectrum. We similarly derive an independent additional value of ΔV_{B-A} from the highest S/N A (+HF) spectrum and a B (+HF) spectrum taken within an hour of that spectrum.

We emphasize that systematic errors in ΔV_{B-A} due to *instrumental* effects should be small since the observations of A and B were taken so close together in time. Table 2 gives the ΔV_{B-A} results with formal errors determined from the quadratic sum of the errors of the appropriate A and B velocities. Our values of ΔV_{B-A} agree with the Fick Observatory value of ΔV_{B-A} within the much larger errors of that result. The ΔV_{B-A} residuals from the various orbits will be discussed below.

4. THE VISUAL-BINARY DATA

We have recomputed the visual-binary orbit of 36 Oph because Orbit 1 was based only on data acquired prior to 1957. Furthermore, the new visual orbit provides a consistent benchmark with which to compare our other orbits that have been constrained by the PRV and the ΔV_{B-A} data.

4.1 Positional Observations Derived from the WDSCO

Worley (1993) has kindly provided observations of 36 Oph in machine-readable form from the *Washington Double Star Catalog of Observations* (WDSCO). This comprehensive data set of visual-binary observations is an invaluable resource that greatly reduces the difficulties in determining visual-binary orbits. From this catalog we have extracted the observation date, the separation ρ (arcsec), the position angle θ (deg) of B relative to A, the number of nights of observation, N, used to calculate the tabulated ρ and θ, the code for the observer or observatory, and the code for the observational method. We corrected one 180 deg er-

ror in position angle. We ignored a total of 12 of the 222 observations in the catalog for the following reasons: we ignored (at Worley's request) observations that were privately communicated to Worley; we also ignored observations where the observing technique was not identified; the separation was an upper limit; or where either the separation or position angle had wild values (deviations greater than 4σ from a preliminary orbit, see below), was not observed, or was marked unreliable in the WDSCO.

The observations were corrected to the J2000 coordinate system using some of the barycentric, precession, and space motion subroutines developed for our PRV studies. The corrections for precession and proper motion are the most important effects as evidenced by the close agreement between our corrections and the simple formulas given by van den Bos (1962).

4.2 Weighting of the WDSCO Observations

The computation of visual-binary orbits requires consideration of the relative weight to assign each observer's measurements. We have developed an objective and reproducible method of assigning weights which we describe here.

We assign preliminary weights using

$$w_\rho = N \tag{1}$$

for the separation observations and

$$w_\theta = (\rho(\pi/180))^2 N \tag{2}$$

for the position-angle observations. The latter equation follows from the assumption that the tangential errors are proportional to the radial (ρ) errors. Define

$$\chi^2/n = \sum_{i=1}^{n} w_i^p r_i^2/n, \tag{3}$$

where, for the ith observation, w_i^p is the preliminary weight calculated from Eq. (1) or (2), r_i is the residual from a preliminary orbit, and n is the number of data points included in the sum. If $n \geq 18$, then χ^2/n is determined with (barely) adequate statistical precision. [Recall that for Gaussian errors the relative standard deviation of χ^2/n is $(2/n)^{1/2} = 1/3$ for 18 observations.] Thus, if a given observer has 18 or more observations, we divide the preliminary weights by χ^2/n where the sum is taken over the ρ or θ observations of that observer. Otherwise, we divide the preliminary weights by χ^2/n, where the sum is taken over *all* the ρ or θ observations of the *kind* of observing technique used by the observer.

Of course, the derived preliminary orbit and thus the residuals used to calculate the weighting depend on the weighting, but only a few iterations are required to get consistent weights to three figures. To reduce the chance of wild values affecting the final results, all (ρ, θ) pairs where one or both of the residuals are $>4\sigma$ are eliminated from further consideration after each iteration. For 36 Oph, the final number of observations is 210 in ρ and 210 in θ. The final adopted χ^2/n values are given in Table 3. We define the final weights and internal errors by

$$w_i = w_i^p/(\chi^2/n) \tag{4}$$

TABLE 3
χ^2/n Values for Visual-Binary Observations

Type	Obs[a]	Tech[b]	n	χ^2/n
ρ	...	A	130	1.21D-01
θ	...	A	130	2.51D-02
ρ	...	B	6	2.19D-01
θ	...	B	6	1.21D-02
ρ	...	D	4	6.43D-02
θ	...	D	4	2.43D-02
ρ	...	G	5	2.29D-03
θ	...	G	5	4.53D-04
ρ	...	H	42	2.11D-04
θ	...	H	42	2.08D-04
ρ	USN	H	20	2.93D-04
θ	USN	H	20	1.77D-04
ρ	...	W	3	9.79D-03
θ	...	W	3	1.34D-03

Notes to TABLE 3

[a]Observatory: USN=United States Naval Observatory.
[b]Technique code assigned by Worley (1993): A=refractor, micrometer; B=reflector, micrometer; D=heliometer; G=photographic, with astrograph; H=photographic, with medium- or long-focus technique; W=area scanner.

and

$$\sigma_i \equiv w_i^{-1/2} = (w_i^p/(\chi^2/n))^{-1/2}, \tag{5}$$

where χ^2/n is the appropriate value taken from Table 3.

We have several comments about these results. (1) Because of the small number of observations made with the B, D, G, and W techniques, the associated weighting for these methods is only reliable in order of magnitude. Nevertheless, we decided to include these data for completeness. (2) The normalization of the preliminary weights [see Eqs. (1) and (2)] is done in such a way that the ratio of derived χ^2/n values for the ρ and θ observations is an estimate of the square of the ratio of the radial and tangential errors. We confirm the well-known effect that the radial errors are larger than the tangential errors for measurements with the visual micrometer (the A technique). On the other hand, one would expect no difference between radial and tangential errors for the photographic technique, and this seems to be confirmed for the H technique within the statistical uncertainties of the derived χ^2/n values. (3) For 36 Oph, observations with the H technique are an order of magnitude more accurate than observations taken with the A technique. It is this wide disparity which forces us to use *nonuniform* weighting for the visual-binary observations of 36 Oph.

5. THE DETERMINATION OF THE ORBIT OF 36 OPH IN THREE DIMENSIONS

Because only a small fraction of the period has been observed and because of the limited precision of the observations, it is impossible to determine the orbit of 36 Oph from observations alone. We must fix the period P (yr) or semimajor axis α (arcsec) using Kepler's third law,

$$\alpha^3/P^2 = (M_A + M_B)\ \pi_P{}^3, \tag{6}$$

where π_P is the absolute parallax (arcsec) and (M_A+M_B) is the sum of the component masses ($M_\odot$). In addition, we determine the spectroscopic-binary amplitude of 36 Oph B relative to A using

$$K_{B-A} \propto ((M_A+M_B)/P)^{1/3} \sin i/\sqrt{1-e^2}, \quad (7)$$

while the component amplitudes are determined from

$$K_A = K_{B-A}/(1+M_A/M_B) \quad (8)$$

and

$$K_B = K_{B-A}/(1+M_B/M_A). \quad (9)$$

5.1 The Component Masses and Parallax

Cayrel de Strobel et al. (1989) have reviewed the mass–luminosity results from stellar interior calculations of the zero-age main sequence (ZAMS). The results for 36 Oph depend on the various models used and can be characterized by an A or B component mass of $0.75 \pm 0.04\ M_\odot$.

For such an important nearby system, the parallax results for 36 Oph are surprisingly meager with errors which are an order of magnitude larger than what is possible for modern parallax studies. Nevertheless, because this system is only 5 parsecs away, the parallax is relatively well determined. The weighted mean of the two relative parallax results converted to absolute is $\pi_P = 0.1874 \pm 0.0093$ arcsec (van Altena 1993).

The calculated values for α^3/P^2 [see Eq. (6)] and K_{B-A} [see Eq. (7)] are affected by the uncertainties in the parallax and the sum of the component masses. If the parallax errors are Gaussian, the 99% confidence interval is $0.1634 \leqslant \pi_P \leqslant 0.2114$ arcsec. For the calculated α^3/P^2 value, these parallax uncertainties dominate the uncertainties in the sum of the component masses. The calculated K_{B-A} value is not directly affected by the parallax uncertainty but is affected by the uncertainty in the sum of the component masses.

5.2 The Orbit Computations

We determine the orbital parameters and their formal errors using the method of least squares. We use the Marquardt technique (Press et al. 1986, hereafter NR) to minimize χ^2, the weighted sum of squares of the residuals. The orbit-fitting technique has been described previously (Papers I and II), and we only mention additional details here that are important in the determination of the 36 Oph orbit.

This orbit has high eccentricity so we fitted the data using the composite parameters α^3/P^2 [frozen at 9.87×10^{-3} $M_\odot$ arcsec^3 consistent with Eq. (6) and the parallax and mass results discussed previously] and $P(1-e)^{3/2}$. These composite parameters remain well defined even in the limit as the eccentricity e approaches unity (see the van den Bos 1962 discussion of parabolic orbits).

It is almost universally advocated (see discussion in Chap. 14 of NR) that the second term of the curvature matrix [Eq. (14.4.7) in NR] should be ignored when calculating the Marquardt step in parameter space. Far from the minimum the second term of the curvature matrix does destabilize the Marquardt technique, and near the minimum the second term should be small relative to the first term. However, for a fit with highly correlated parameters small changes in the curvature matrix make large changes in the size and direction of the Marquardt step. In fact, we have found that the later stages of the Marquardt convergence are substantially accelerated if we employ the second term in the curvature matrix. The required second partial derivatives of the fitting function can be calculated rapidly from formulas determined by analytical differentiation of the orbit-fitting functions. Inclusion of the second term in the curvature matrix makes its components exact partial derivatives of the components of the gradient vector. Thus, the later stages of the Marquardt technique converge quadratically in the parameters and quartically (!) in χ^2. This makes it easy to recognize when the χ^2 minimum has been reached, if we employ a tight convergence criterion. (The iterations are stopped only when the relative change in χ^2 is less than 1 part in 10^7.) Once the minimum has been found, it is easy to show that the formal errors and correlation matrix must be determined from the inverse of the curvature matrix calculated with the second term *dropped*. Thus, the formal errors and correlation matrix are calculated with the same formulas that are used for linear least squares.

6. RESULTS

6.1 The Derived Orbits

Table 4 compares parameters of the 36 Oph orbit determined from various assumptions. Orbit 1 (=Orbit II of Brosche 1960) was determined from visual-binary observations taken prior to 1957. Assuming the 30 Brosche normal points represent all the pre-1957 data in the WDSCO, this orbit only represents about 70% of the WDSCO observations and only about one-third of the high-quality observations determined with the photographic technique. Orbit 2 was determined in the present work from a weighted least-squares fit of the visual-binary data from WDSCO. Orbit 3 was determined from a simultaneous fit of the visual-binary data and the PRV data for 36 Oph A and B. We show below that the orbit results are insensitive to assumed mass ratio. Because of the virtually identical photometric and spectroscopic properties of the two stars, we have assumed $M_B/M_A = 1$ which, in turn, implies that the spectroscopic-binary amplitudes of A and B are given by $K_A = K_{B-A}/2$ and $K_B = K_{B-A}/2$ [see Eqs. (8) and (9)]. For the spectroscopic-binary fitting functions we take $\omega_B \equiv \omega$ and $\omega_A \equiv \omega + 180$ deg, where ω is given in Table 4. We set the PRV weights equal to the inverse square of the internal errors. The PRV data are *differential* with the weighted mean velocity arbitrarily set to zero for both the 36 Oph A and 36 Oph B data sets. Thus, the Orbit 3 fit included the determination of arbitrary independent zero points for the two sets of PRV data. Orbit 4 was determined from a simultaneous fit of the visual-binary data, the PRV data, and the ΔV_{B-A} values given in Table 2. We set the ΔV_{B-A} weights equal to the inverse square of the formal errors given in Table 2.

Because of the high correlation between the derived parameters, certain linear combinations of the parameters are much better determined than the parameters themselves, and we must include up to five guard digits in the fitted param-

TABLE 4
Orbits for 36 Oph AB

Parameter	Units	Orbit 1[a]	Orbit 2[b]	Orbit 3[c]	Orbit 4[d]
α	arcsec	13.91	13.0	13.1	14.7
		...	...	...	...
α^3/P^{2e}	$M_\odot$ arcsec^3	8.9395D-3	9.87D-03	9.87D-03	9.87D-03
		...	...	...	...
i	deg	99.18	99.794157	99.742431	99.55519
		...	0.21	0.22	0.12
ω	deg	-90.	-90.19976	-91.09975	-83.58765
		...	2.4	1.6	0.11
Ω	deg	-86.36	-85.84473	-83.2017	-104.91748
		...	7.1	4.2	0.41
e	...	0.9	0.91592197	0.91568808	0.9223699
		...	0.0017	0.0014	0.0011
T^f	dy	-118672.	-106115.4	-113064.2	-74874.8
		...	18000.	14000.	1500.
T	yr	1643.48	1677.86	1658.83	1763.39
		...	...	...	...
P	yr	548.7	470.9	476.5	568.9
		...	...	...	...
$P(1-e)^{3/2}$	dy	6337.5	4193.516	4260.544	4494.58
		...	270.	300.	180.
$K_{B-A}{}^g$	m s^{-1}	...	...	10705.	10503.
		...	...	...	...
$\gamma_A{}^h$	m s^{-1}	...	...	-749.60	317.812
		...	...	210.	7.0
$\gamma_B{}^i$	m s^{-1}	...	...	740.854	-323.846
		...	...	210.	7.0
χ^2/n^j	...	2.413	0.996	0.996	1.021

[a]Orbit II from Brosche 1960.
[b]Fit (this work) of the WDSCO visual-binary data.
[c]Same as Orbit 2 except the PRV data for 36 Oph A and B with arbitrary zero points are also simultaneously fitted.
[d]Same as Orbit 3 except the observed ΔV_{B-A} values (Table 2) are also simultaneously fitted.
[e]$\alpha^3/P^2 = (M_A + M_B)\pi_P{}^3$ is fixed by the adopted $M_A + M_B = 1.5M_\odot$ and $\pi_P = 0.1874$ arcsec for Orbits 2, 3, and 4 (see text).
[f]$RJD = JD - 2440000$.
[g]Spectroscopic binary amplitude calculated from the adopted $M_A + M_B = 1.5M_\odot$ and Eq. (7). $K_A = K_B = K_{B-A}/2$ was calculated from the adopted mass ratio of unity (see Eqs. (8) and (9)).
[h]This system velocity for the A component has an arbitrary zero point (see text).
[i]This system velocity for the B component has an arbitrary zero point (see text).
[j]χ^2/n calculated for *just* the visual-binary data.

Notes to Table 4.

For each parameter, the first row is the value and second row the formal error (see text). The 180 deg ambiguity of ω and Ω has been resolved so that ω is the B (secondary) longitude of periastron, Ω is the position angle of the *ascending* node, and the correct sign is predicted for the A and B accelerations (Table 1).

eters of Table 4 to preserve the χ^2 value to our convergence criterion (1 part in 10^7). Any significant reduction in the guard digits runs the risk of moving the solution outside of the quartic convergence region of χ^2 (see previous discussion).

The χ^2/n value [calculated with final weights, see Eq.(4)] for *only* the visual-binary data is given in the last row of Table 4 and indicates the relative quality of the visual-binary fits. Orbit 1 is of poorer quality because it was based only on older observations; it almost inevitably shows some small systematic deviations from the modern visual-binary observations. Orbits 2 and 3 are quite similar, but Orbit 4 fits the visual-binary data almost equally well. Figure 2 shows the residuals from Orbit 4. The systematic deviations appearing in both ρ and θ for the early data are present for all orbits and probably indicate that there are small systematic errors in the visual-binary data.

Orbit 4 differs substantially from the other orbits (see Figs. 3 and 4). For example, the eccentricity deviates by almost 4σ between Orbits 2 and 4. This is apparently not a case of a multiple solution; if the PRV and ΔV_{B-A} constraints are dropped, the Marquardt technique moves an initial Orbit 4 solution smoothly back to Orbit 2. Presumably the nonlinearities of the fitting function make the χ^2 surface of *just* the visual-binary data similar to a curved shallow valley. This shape allows relatively large visual-binary parameter changes with little change in the associated χ^2 (see also the discussion in Paper I). To make the orbit more reli-

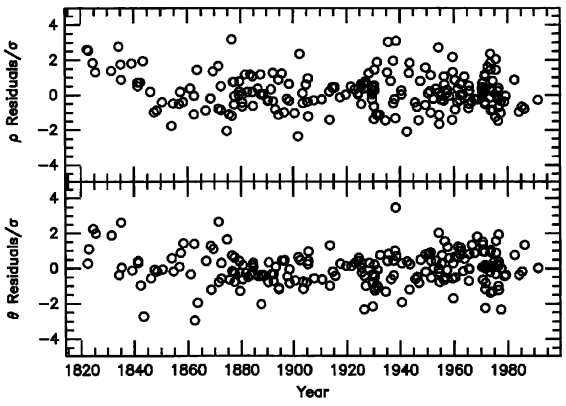

FIG. 2—Visual-binary (ρ and θ) residuals from Orbit 4 of Table 4. We have rendered all residuals on a common dispersion scale by dividing by the appropriate internal errors [see Eq. (5) and Table 3].

able it is essential to employ the additional constraints used for Orbit 3 and especially for Orbit 4.

Figure 4 shows that the predicted radial acceleration of 36 Oph B relative to A is roughly constant in the present era, and this makes it insensitive to parameter changes (see also Table 1). Since the unconstrained Orbit 2 already predicts an acceleration that is approximately correct, the PRV data actually provide little additional constraint, and the Orbit 3 parameters and their formal errors are similar to those of Orbit 2. In contrast, the observations of ΔV_{B-A} greatly constrain Orbit 4, and the formal errors of the parameters are reduced by up to an order of magnitude when compared to the formal errors of Orbits 2 and 3. Orbit 4 does a worse job than the other orbits of predicting the B–A acceleration (see last row of Table 1), but this is a much smaller discrepancy (2.5σ) than the $\sim 100\sigma$ discrepancies between the observed ΔV_{B-A} values and the predictions of the other orbits (see Table 2). For this reason, we reject Orbits 1, 2, and 3 in favor of Orbit 4 for all subsequent analysis.

6.2 Maximum Allowed Companion Mass

Our technique for determining the maximum companion mass from PRV data (see the appendix in WWILYR) can be adapted to derive the maximum companion mass from the visual-binary residuals from Orbit 4. These residuals and the corresponding weights were transformed to the $X \equiv \rho \cos\theta$ and $Y \equiv \rho \sin\theta$ coordinate system. According to the numerical simulations the weighted periodograms (not illustrated) of the X and Y residuals showed no peaks exceeding the 99% confidence limit for periods from 5 to 100 yr. To finish these simulations in a reasonable length of computer time, we have used the weighted periodogram [see Irwin et al. 1989, Eq. (5)] rather than the correlated periodogram [see WWILYR, Eq. (A2)]. We judge that correlation effects between the long-period visual-binary orbit model and the sinusoid model associated with the periodogram calculation should not be important for periodogram periods which are short compared to the observed visual-binary epoch range of 170 yr.

We calculate the maximum (upper-tailed 99% confidence limit) periodic amplitude allowed by the visual-binary residuals from Orbit 4 following WWILYR. The combination of the properly phased X and Y maximum-amplitude sinusoids results in an apparent ellipse on the sky. The maximum total amplitude α_{max} is the semimajor axis of this ellipse which we transform to maximum allowed companion mass m (Jupiter masses) using

$$m = 1.05 \times 10^3 (\alpha_{max} / \pi_P)(M_* / P)^{2/3} \qquad (10)$$

[see Campbell et al. 1988, Eq. (7)]. In these equations P is measured in yr, α_{max} is measured in arcsec, and the component mass M_* is measured in solar masses.

Figure 5 gives the maximum companion mass to either 36 Oph A or B allowed by the visual-binary residuals from Orbit 4 for assumed periods from 5 to 100 yr. The basic assumptions of this calculation are the actual eccentricity (not the apparent eccentricity which involves the orbital inclination) of the possible companion orbit is small, and any other effect (e.g., systematic errors in the visual-binary data) does not subtract out a *larger* orbital variation by accident.

For periods from 5 to about 50 yr the visual-binary data [especially those taken with the photographic technique (see H in Table 3)] have sufficient accuracy to limit α_{max} to less than 20 milliarcsec. Beyond 50 yr we must rely on the much

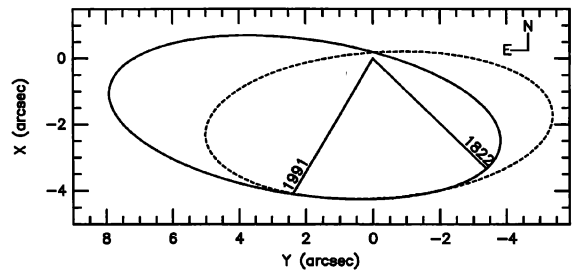

FIG. 3—Two predicted visual-binary orbits of 36 Oph B relative to A which virtually coincide over the range of observed motion from 1822 to 1991. The limits of the observed motion are marked by radial lines from the origin. Orbit 2 of Table 4 is marked by a dashed line; Orbit 4 of Table 4 is marked by a solid line.

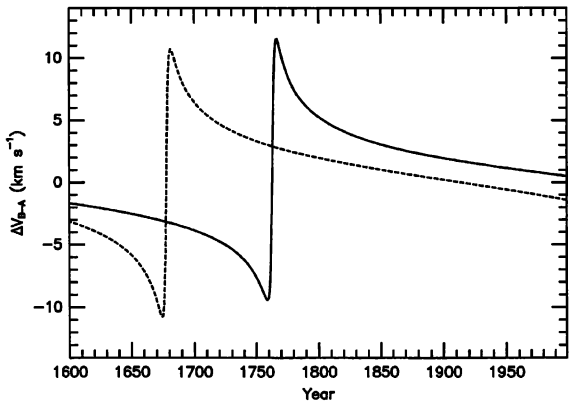

FIG. 4—Two predicted ΔV_{B-A} orbits of 36 Oph AB. Orbit 2 of Table 4 is marked by a dashed line; Orbit 4 of Table 4 is marked by a solid line. In the modern era the predicted B–A acceleration is insensitive to orbit parameter changes. On the other hand, Orbit 4 gives an excellent prediction of ΔV_{B-A} while the remaining orbits do not (see Table 2).

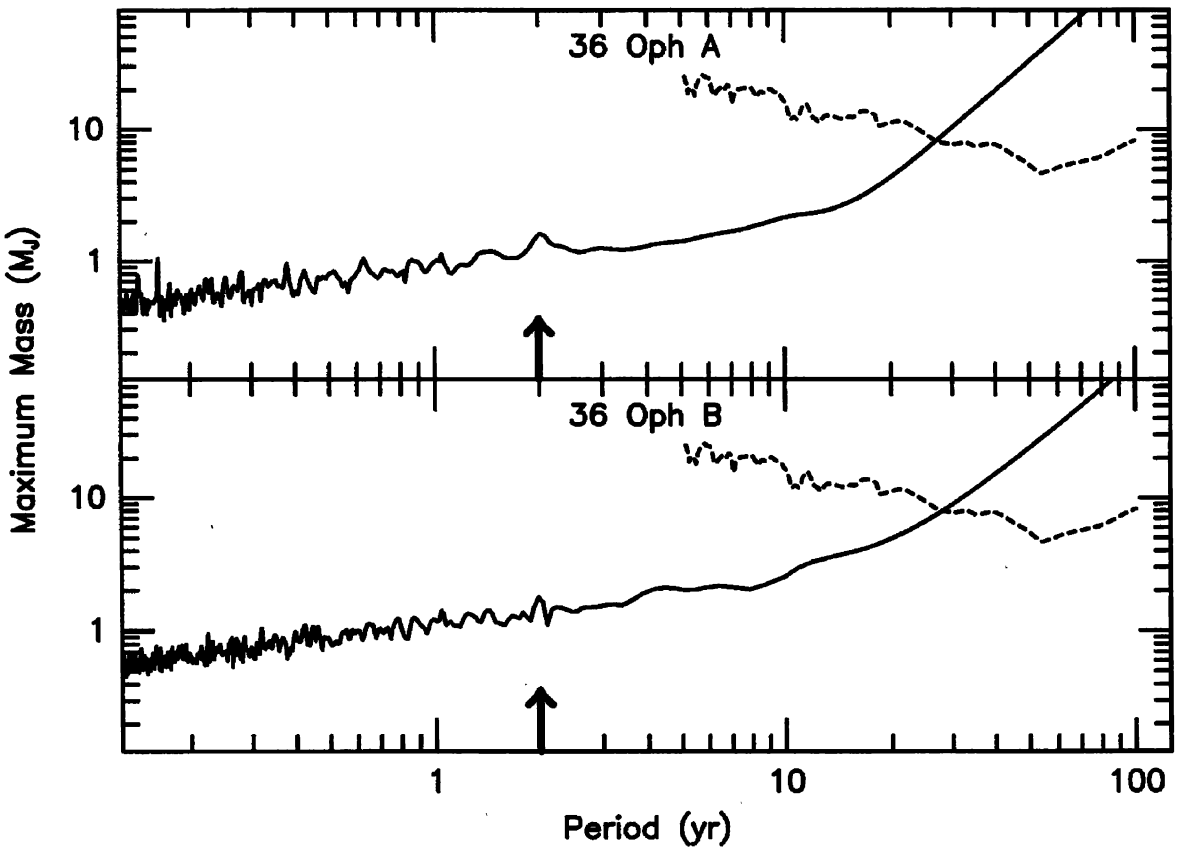

FIG. 5—Maximum companion mass allowed by the visual-binary and PRV residuals from Orbit 4 of Table 4. The visual-binary mass limit (dashed line) is the same for 36 Oph A and B and is calculated from Eq. (10) and the maximum total amplitude α_{max} allowed by the visual-binary residuals (see text). The PRV mass limits ($\times \sin i$) are plotted as solid lines and are determined from an analysis of the PRV residuals (WWILYR). The arrows in the figure correspond to the maximum companion period allowed by a dynamical stability argument; see Sec. 6.3.

less accurate visual-micrometer technique (see A in Table 3) to limit the maximum companion mass. This causes the increase of the maximum companion mass allowed by the visual-binary data for periods longer than 50 yr.

Figure 5 also illustrates the maximum companion mass ($\times \sin i$) derived from an analysis of the PRV Orbit 4 residuals (WWILYR) for periods from 40 dy to 100 yr. The PRV and visual-binary results nicely complement each other and lead to the conclusion that *from observational constraints alone* the maximum allowed companion mass to 36 Oph A or B is of order 8 Jupiter masses for assumed periods near 30 yr with smaller mass limits ($\times \sin i$) for shorter periods and also smaller mass limits for longer periods. An orbital instability argument (next subsection) constrains the maximum companion mass still further.

6.3 The Period Limit Due to Orbital Instability

For the case of a substellar companion to one member of a binary system, there is a limit on the maximum size of the semimajor axis and period of the hypothesized substellar companion orbit. For 36 Oph B this period limit is short enough so that the maximum mass derived in the previous section can be further constrained. In addition this period limit can be used to rule out a substellar companion as the cause of the acceleration residual.

A key parameter in orbital stability analysis is $Q=a(1-e)/a_c$, where $a(1-e)$ is the binary distance of closest approach, $a_c \approx M_*^{1/3} P_c^{2/3}$ is the semimajor axis of the hypothesized substellar companion orbit about one of the binary stars, and P_c is the corresponding companion period. For binary mass ratios near unity, Q must be generally greater than about 4 for orbital stability (see Donnison and Mikulskis 1992, Figs. 5 and 6). From the parameters of Orbit 4, this corresponds to a maximum a_c value of 1.5 a.u. or maximum P_c of 2 yr. This maximum companion period is some 300 times smaller than the binary period because the large binary eccentricity forces the distance of closest approach to be much smaller than the binary semimajor axis. This general stability analysis has been confirmed for the specific orbit of 36 Oph using three-body orbit calculations (Krymolowski and Mazeh 1995). The maximum companion period allowed for stable orbits is marked in Fig. 5 with a vertical arrow and corresponds to a maximum companion mass ($\times \sin i$) of about 2 Jupiter masses for both 36 Oph A and B. This period limit also means the long-term accel-

eration residual of 36 Oph B cannot be due to a substellar companion.

7. DISCUSSION

7.1 Possible Deviations Between ΔV_{B-A} and the Center-of-Mass Velocity Difference

The results of this paper depend on the assumption that the measured value of ΔV_{B-A} corresponds to the difference in radial velocity between the centers of mass of 36 Oph A and B. In this subsection we discuss the validity of this assumption.

The usual PRV technique effectively compares differential line velocities observed at different epochs for the *same* star. Therefore, if the stellar spectrum remains constant with time, then constant blending shifts and convective blueshifts should subtract out for each line and add no noise to the PRV results. On the other hand, the technique for obtaining ΔV_{B-A} necessarily means we must compare line velocities taken for two *different* stars. For the case of 36 Oph A and B, we are lucky that the spectra are virtually identical so that the ΔV_{B-A} error (see Table 2) is virtually identical to the error expected from the ordinary PRV technique. The small random errors of the two independent ΔV_{B-A} results in Table 2 are confirmed by the difference of only 19 m s^{-1} between the ΔV_{B-A} values corrected for the mean observed acceleration (Table 1) of B relative to A.

We expect the gravitational redshift and mean convective blueshift to have a negligible systematic effect on the observed ΔV_{B-A} values. The mass and radius, and, therefore, the gravitational redshift should be virtually identical for the two stars. The mean convective blueshift is caused by the intensity contrast between hot rising elements and cool falling elements and is of order 300 m s^{-1} for the blue solar spectrum. However, convective blueshifts should be weaker at our long observing wavelengths (870 nm), and presumably there is cancellation of similar effects for 36 Oph A and B. Finally, the effect should vary with line strength and thus introduce excess dispersion in the velocities. In fact, the excess dispersion is indiscernible so we conclude that the systematic convective blueshift effect on ΔV_{B-A} is of the order of the internal errors of ΔV_{B-A} or smaller.

7.2 The Reliability of the Orbit 4 Acceleration Predictions

Orbit 4 is consistent with the theoretical mass–luminosity relation and also the observed parallax, ΔV_{B-A}, and 36 Oph A acceleration. However, the Orbit 4 B–A and B acceleration predictions would have to be increased respectively by factors of 1.40 and 1.64 to agree with the observations (see Table 1).

These discrepancies cannot be attributed to uncertainties in the sum of masses, parallax, or mass ratio that were adopted for the fit. If we vary the adopted sum of masses through twice the range of known theoretical results ($1.34 \leq M_A + M_B \leq 1.66\ M_\odot$; see Sec. 5.1) the predicted B–A acceleration changes by ± 50 m s^{-1} Jcy^{-1}, only 1/10th of the required change. Clearly, the sum of mass change required to account for the whole B–A acceleration discrepancy would be completely discordant with the observed luminosities, colors, and spectral types of 36 Oph A and B. The spectroscopic-binary amplitude [K_{B-A}, see Eq. (7)] and the predicted B–A acceleration depend on the orbit parameters which in turn are affected by the parallax adopted for the fit. However, because the effect is indirect, the predicted B–A acceleration is insensitive to the adopted parallax; a variation of the adopted parallax through its 99% confidence interval ($0.1634 \leq \pi_P \leq 0.2114$ arcsec) causes the predicted B–A acceleration to vary by less than ± 5 m s^{-1} Jcy^{-1}, only 1/100th of the required change. The predicted B–A acceleration is also indirectly affected by the adopted mass ratio through the influence of the PRV data on the derived orbital parameters. However, a change in the adopted mass ratio affects the 36 Oph A and B PRV fits in opposite senses [see Eqs. (8) and (9)] so the net effect on the orbit and predicted B–A acceleration is quite small. Changing the adopted mass ratio from $M_B/M_A = 1$ to 0.75 (a value grossly discordant with the ZAMS model results and the virtually identical photometric and spectroscopic properties of 36 Oph A and B) changes the B–A acceleration by only 1 m s^{-1} Jcy^{-1}. Of course, K_A, K_B, and the predicted *component* accelerations depend directly on the adopted mass ratio [see Eqs. (8) and (9)], but the effect is simply to redistribute the factor-of-1.40 B–A acceleration discrepancy various ways among the component accelerations. For example, even if we adopt $M_B/M_A = 0.75$, the B acceleration discrepancy is only reduced from a factor of 1.64 to 1.44.

Our orbit and predicted accelerations are critically dependent on the 22 visual-binary observations prior to 1860, but unacceptably large systematic errors would be required in these early data even to partially resolve the acceleration discrepancy. For example, we were able to reduce the 36 Oph B acceleration discrepancy from a factor of 1.64 to 1.3 by arbitrarily increasing the PRV weights by a factor of 100 in the fit. However, the residuals of the early observations from this test orbit show systematic secular trends that approach 5 deg in position angle and 2 arcsec (approximate observed and predicted separations are about 5 and 3 arcsec, respectively) at the earliest epoch. The early observers can be checked by comparing their observations for ξ Bootis, for example, with modern observations taken one period later. There is no sign of the large systematic deviations that occur for the 36 Oph test orbit.

It is unlikely that a systematic deviation between the measured ΔV_{B-A} values and the actual center-of-mass velocity difference is large enough to have any significant effect on the predicted orbit accelerations. Clearly, a 2 km s^{-1} systematic change in ΔV_{B-A} could resolve the discrepancy (see Orbit 3, Tables 1 and 2), but we feel an instrumental error, gravitational-redshift difference, or convective-blueshift difference of this order is not possible (see the discussion in the previous subsection). We acknowledge the possibility of systematic errors in the visual-binary and PRV observations that are the order of the internal errors. However, it is unlikely that systematic errors of this order in the two kinds of data would have an important effect on the predicted acceleration of Orbit 4. The ΔV_{B-A} constraint is just too powerful. Substantial perturbations of Orbit 4 (see the above sum of mass,

parallax, mass ratio, and weight perturbations) leave the predicted acceleration little changed, and we expect similar robustness against systematic errors.

8. CONCLUSIONS

The 36 Oph A and B observations were part of a larger program that monitored the precise radial velocities of 21 dwarfs and subgiants from 1980 to 1992 at the CFHT. Six of these stars including 36 Oph B have demonstrated significant (false-alarm probability <0.01) unexplained trends in their radial velocities (WWILYR, Table II; see also Campbell et al. 1988). We do not believe the trends are of instrumental origin since we also measured a number of stars which were constant.

At the time of writing, six dwarf stars have been discovered to have low-amplitude, periodic variations in their radial velocity that may indicate the presence of substellar companions. These stars [HD 114762, HD 140913, and HD 29587 (Mazeh et al. 1996); 51 Pegasi (Mayor and Queloz 1995); 47 Ursae Majoris (Butler and Marcy 1996); and 70 Virginis (Marcy and Butler 1996)] show a wide range of periods from 4.2 dy to 4 yr. As the radial-velocity searches continue, longer-period substellar candidates will undoubtedly be discovered. The discovery of the periodic candidates adds some strength to the case that at least some of the secular trends we have discovered are caused by substellar companions with periods exceeding 15 yr and maximum allowed masses ($\times \sin i$) of 3–10 Jupiter masses (WWILYR).

However, the case of 36 Oph B is an important counterexample that serves as a warning that not all these unexplained trends can be due to a substellar companion. The residuals from the orbit prediction cannot be explained by any reasonable variation in the orbital parameters, and the high eccentricity of the stellar binary orbit assures a close approach that would disrupt any substellar companion to B (or A) with a period exceeding approximately 2 yr.

What then are the possible explanations of the systematic residuals in the 36 Oph B velocities?

(1) We can immediately dismiss a global acceleration of the stellar surface in all the cases where we have discovered a secular trend. For example, 36 Oph B cannot sustain a surface acceleration of 400 m s^{-1} Jcy^{-1} $\approx 0.2\ R_\odot$ yr^{-2} for very long.

(2) For 36 Oph, we might be the victim of systematic errors in the visual-binary observations prior to 1860. Our orbit does depend critically on these early data, but our tests indicate unacceptably large systematic errors would be required in these data to even partially resolve the systematic residuals in the velocities.

(3) We might be the victim of systematic errors in the 36 Oph B PRV data prior to 1983. Clearly, the early PRV data are driving the acceleration discrepancy for 36 Oph B; the acceleration of the post-1983 data for 36 Oph B is -750 ± 160 m s^{-1} Jcy^{-1}, which is in reasonable accord with the Orbit 4 predictions (see Table 1). However, we see no general systematic errors in the other stars we have monitored; the majority are constant, and, in particular, the extensive data prior to 1983 for τ Ceti show systematic deviations which are much less than the required 50 m s^{-1} (see WWILYR, Fig. 1). Nevertheless, it is important for the other PRV groups to continue to monitor 36 Oph B to see whether the acceleration discrepancy continues.

(4) The radial velocity may *partially* correlate with chromospheric activity. A sudden decrease of 50 m s^{-1} in the surface velocity of 36 Oph B may have occurred in 1983 to mimic a long-term trend. Such a sudden decrease seems to correlate with the decrease in chromospheric emission that occurred for this star in 1983 (see Fig. 1). For κ^1 Ceti (G5 V) an episode of large chromospheric emission was coincident with an apparent increase of the radial velocity (see Fig. 1 of WWILYR). It is known (see Basri et al. 1989) that an increase in chromospheric activity can lead to a filling in of the core of lines which are much weaker than the strong lines whose cores are traditionally used to measure chromospheric activity. It is possible this filling in of weak lines is accompanied by a shift in PRV results which are also determined from the weaker lines. (The 866.2 nm line of Ca II is excluded from our PRV results.) However, if the velocity shift occurs, it does not necessarily occur for every episode of chromospheric activity. For example, the steep drop and rise of chromospheric activity that occurs near 1990 seems to have no effect on the velocity residuals of 36 Oph B. Furthermore, there seems to be no velocity effect for 36 Oph A although its chromospheric activity range and mean level (recall that the $\Delta EW_{866.2}$ plots in Fig. 1 have a common zero point) is similar to that of 36 Oph B. Perhaps the shorter-term nature of the variations in the chromospheric activity of 36 Oph A has something to do with the lack of velocity variations for that star. Clearly, more work needs to be done to investigate the possible connection between PRV shifts and certain kinds of chromospheric activity.

(5) The convective blueshift may vary with time. The temperature difference between rising and falling elements may change and/or the mean velocities of rising and falling elements may change. Note the effect required is of order 50 m s^{-1}. Thus if this proves to be the explanation, it would only have a minor effect on the measured ΔV_{B-A} values and the derived orbit. A convective blueshift that varies with time could explain any or all of the secular trends or short-term variations we have discovered but begs further questions about the physical mechanism, the reason why most stars do not show the phenomenon, and the connection (if any) with chromospheric activity. If the convective blue shift does change significantly with time, then the effect should be larger at the shorter wavelengths where the other PRV groups observe. Clearly, it is important to continue to monitor the dwarf stars to see whether the radial acceleration discrepancies we have found depend on observing wavelength.

We would like to thank all those who helped with this research. Bruce Campbell made many important contributions before he left the PRV program in 1990. Cherie Goodenough, Ana Larson, David Bohlender, and Andrew Walker provided research assistance. Don VandenBerg gave financial support. Charles Worley and William van Altena have privately communicated results from their extremely useful catalogs. Jim Hesser provided facilities at the Dominion Astrophysical Observatory (to A.W.I.) where a portion of this

research was completed. Tsevi Mazeh reminded us that dynamical instability imposes maximum periods for substellar companions to binary stars and Yuval Krymolowski and Tsevi Mazeh privately communicated their three-body calculations which established this limit for 36 Oph. This research has made use of the SIMBAD data base, operated at CDS, Strasbourg, France. This research was supported in part by grants from the Natural Sciences and Engineering Research Council of Canada to Bruce Campbell, Gordon Walker, and Don VandenBerg.

REFERENCES

Basri, G., Wilcots, E., and Stout, N. 1989, PASP, 101, 528
Beavers, W. I., and Eitter, J. J. 1986, ApJS, 62, 147
Brosche, P. 1960, Astron. Nach., 285, 261
Butler, R. P., and Marcy, G. W. 1996, ApJ (in press)
Campbell, B., and Walker, G. A. H. 1979, PASP, 91, 540
Campbell, B., Walker, G. A. H., and Yang, S. 1988, ApJ, 331, 902
Cayrel de Strobel, G., Perrin, M.-N., Cayrel, R., and Lebreton, Y. 1989, A&A, 225, 369
Donnison, J. R., and Mikulskis, D. F. 1992, MNRAS, 254, 21
Hoffleit, D., and Warren, W. 1991, The Bright Star Catalogue, 5th ed. on-line version in L. E. Brotzmann and S. E. Gessner, The Astronomical Data Center CD-ROM Selected Astronomical Catalogs, Volume I, Doc. No. STX-T-1-5002-009-91, NASA, Goddard Space Flight Center (ST Systems Corp.)
Irwin, A. W., Campbell, B., Morbey, C. L., Walker, G. A. H., and Yang, S. 1989, PASP, 101, 147
Irwin, A. W., Yang, S., and Walker, G. A. H. 1992a, PASP, 104, 101 (Paper I)
Irwin, A. W., Fletcher, J. M., Yang, S. L. S, Walker, G. A. H., and Goodenough, C. 1992b, PASP, 104, 489 (Paper II)
Krymolowski Y., and Mazeh T. 1995, private communication
Larson, A. M., Irwin, A. W., Yang, S. L. S., Goodenough, C., Walker, G. A. H., Walker, A. R., and Bohlender, D. A. 1993a, PASP, 105, 332
Larson, A. M., Irwin, A. W., Yang, S. L. S., Goodenough, C., Walker, G. A. H., Walker, A. R., and Bohlender, D. A. 1993b, PASP, 105, 825
Marcy, G. W., and Butler, R. P. 1996, ApJ (in press)
Mayor, M., and Queloz, D. 1995, Nature, 378, 355
Mazeh, T., Latham, D. W., and Stefanik, R. P. 1996, ApJ (in press)
Press, W. H., Flannery, B. P., Teukolsky, S. A., and Vetterling, W. T. 1986, Numerical Recipes (Cambridge, Cambridge University Press) (NR)
van Altena, W. F. 1993, private communication of preliminary results from The General Catalog of Trigonometric Stellar Parallaxes
van de Kamp, P. 1981, Stellar Paths (Dordrecht, Reidel)
van den Bos, W. H. 1962, in Astronomical Techniques, ed. W.A. Hiltner (Chicago, University of Chicago Press), Chap. 22
Walker, G. A. H., Walker, A. R., Irwin, A. W., Larson, A. M., Yang, S. L. S., and Richardson, D. C. 1995, Icarus, 116, 359 (WWILYR)
Worley, C. E., and Heintz, W. D. 1991, Fourth Catalog of Orbits of Visual Binary Stars, in L. E. Brotzmann and S. E. Gessner, The Astronomical Data Center CD-ROM Selected Astronomical Catalogs, Volume I, Doc. No. STX-T-1-5002-009-91, NASA, Goddard Space Flight Center (ST Systems Corp.)
Worley, C. E. 1993, private communication of results from the Washington Double Star Catalog of Observations (WDSCO)